

Research Paper

Localized injection of miRNA-21-enriched extracellular vesicles effectively restores cardiac function after myocardial infarction

Yu Song^{1*}, Cheng Zhang^{1,2*}, Jinxiang Zhang^{3*}, Zhanying Jiao¹, Nianguo Dong⁴✉, Guobin Wang²✉, Zheng Wang^{1,2}✉, Lin Wang^{1,5}✉

1. Research Center for Tissue Engineering and Regenerative Medicine, Union Hospital, Tongji Medical College, Huazhong University of Science and Technology, Wuhan, 430022, China
2. Department of Gastrointestinal Surgery, Union Hospital, Tongji Medical College, Huazhong University of Science and Technology, Wuhan, 430022, China
3. Department of Emergency Surgery, Union Hospital, Tongji Medical College, Huazhong University of Science and Technology, Wuhan, 430022, China
4. Department of Cardiovascular Surgery, Union Hospital, Tongji Medical College, Huazhong University of Science and Technology, Wuhan, 430022, China
5. Department of Clinical Laboratory, Union Hospital, Tongji Medical College, Huazhong University of Science and Technology, Wuhan, 430022, China

*, These authors contributed equally to this work.

✉ Corresponding authors: Phone: 86-27-85726612, E-mail: lin_wang@hust.edu.cn (L. Wang); zhengwang@hust.edu.cn (Z. Wang); wgb@hust.edu.cn (G. Wang); dongnianguo@hotmail.com (N. Dong)

© Ivyspring International Publisher. This is an open access article distributed under the terms of the Creative Commons Attribution (CC BY-NC) license (<https://creativecommons.org/licenses/by-nc/4.0/>). See <http://ivyspring.com/terms> for full terms and conditions.

Received: 2018.09.14; Accepted: 2019.02.14; Published: 2019.04.13

Abstract

Myocardial infarction (MI), a main cause of heart failure, leads to irreversible cardiomyocytes loss and cardiac function impairment. Current clinical treatments for MI are largely ineffective as they mostly aim to alleviate symptoms rather than repairing the injured myocardium. Thus, development of more effective therapies is compelling. This study aims to investigate whether the extracellular vesicles (EVs) carrying specific anti-apoptotic miRNA can be efficiently internalized into myocardium to achieve desired therapeutic outcomes.

Methods: EVs were isolated from HEK293T cells overexpressing miRNA-21 (miR21-EVs) and identified. The RNase resistant rate of miR21-EVs was calculated by real-time PCR and compared with liposomes and polyethylenimine (PEI). Confocal laser scanning microscopy was used for visualizing the cellular internalization of miR21-EVs in primary cultured mouse neonatal cardiomyocytes (CMs), H9c2 rat cardiomyoblasts, and human umbilical vein endothelial cells (HUVECs). The effect of miR21-EVs on the expression of PDCD4, a pro-apoptotic protein that plays an important role in regulating myocardial apoptosis, was also evaluated in these three cell types by real-time PCR and Western blot analysis. *In vivo*, miR21-EVs was directly injected into the infarct zone following ligation of the left anterior descending of coronary artery in mice. The miR21-EVs distribution and blood vessel (capillary and arteriole) density were evaluated by immunofluorescence staining. Fluorescence in situ hybridization of miRNA-21 was also carried out to confirm the miR21-EVs distribution *in vitro* and *in vivo*. The protein level of PDCD4 in myocardium was assessed by immunohistochemical staining. The anti-apoptotic effect of miR21-EVs in cardiomyocytes and endothelial cells were measured using TUNEL staining. Four weeks after injection, the cardiac histological and functional recovery was evaluated by histochemistry staining and echocardiography, respectively.

Results: In contrast to liposomes and PEI, EVs significantly inhibited miRNA-21 degradation. MiR21-EVs efficiently delivered miRNA-21 into cardiomyocytes and endothelial cells within 4 hours. Exogenous miRNA-21 in turn significantly reduced PDCD4 expression and attenuated cell apoptosis *in vitro*. Consistently and importantly, in a preclinical MI animal model, miRNA-21-loaded EVs effectively sent miRNA-21 into cardiomyocytes and endothelial cells, drastically inhibited cell apoptosis and led to significant cardiac function improvement.

Conclusion: Our results suggest the cell-derived, genetically engineered EVs may be used therapeutically for the delivery of miRNAs for the rescue of MI and may benefit patients in the future.

Key words: extracellular vesicles, miRNA-21, myocardial infarction, functional recovery

Introduction

Ischaemic heart disease is a leading cause of death worldwide [1]. As an ischemic heart disease, acute myocardial infarction (MI) often results in poor outcomes [2]. The occlusion of coronary vessels causes hypoxia, leading to a significant loss of cardiomyocytes, which is often irreversible. Current treatments including surgical interventions and thrombolysis can induce additional reperfusion injury, involving cardiomyocyte death and microvasculature damage [3, 4]. Due to insufficient regenerative capability of remaining cardiomyocytes [5], it is essential to develop effective alternatives for treating MI while reducing cardiomyocyte loss.

Recently, microRNAs (miRNAs) have been explored in treating cardiovascular diseases (CVDs) [6, 7]. MiRNAs are a class of small noncoding RNAs that modulate gene expression by base pairing with 3' untranslated regions (UTR) of targeted mRNAs, which in turn causes mRNA degradation or translational repression [8]. An increasing number of studies show that miRNAs are involved in the regulation of post-MI cardiac angiogenesis, apoptosis, and fibrosis, making them potential pharmacological candidates for MI treatment [9]. However, insufficient stability and poor cellular uptake *in vivo* restrict miRNAs' clinical application [10]. Although several approaches, such as hydrodynamic injection, viral vectors, liposomes and nanocarriers have been developed to deliver miRNAs, these approaches are associated with vehicle toxicity, low efficiency of delivery, and adverse immune reactions. Thus, reliable and efficient delivery approaches are highly desired.

Extracellular vesicles (EVs), a heterogeneous group of cell-secreted structures with diameters ranging from 30-1000 nm [11], have lipid membrane structure similar to liposomes. The robustness of EVs' membrane [12] not only effectively protects nuclei acid cargos of interest from degradation, but also rapidly transport miRNA, mRNA, and proteins into recipient cells without inducing toxicity and adverse immune reactions [13]. MiRNAs within the EVs can be modified to meet the requirement for treating different diseases by either preconditioning or genetic engineering [13, 14]. Thus, EVs may be an optimal choice for miRNA delivery *in vivo*. To date, EVs have been increasingly investigated as biomarkers in CVDs [15] and EVs isolated from various kinds of stem cells, including mesenchymal stem cells (MSCs) [16], cardiac progenitor cells (CPCs) [17], embryonic stem cells (ESCs) [18], and induced pluripotent stem cells (iPSCs) [19], were studied for cardiac repair. However, the passage numbers of stem cells are limited and the yield of EVs are usually very low,

restricting the widely use of EVs for research and clinical therapy. These limitations might be overcome by increasing the yield of EVs from immortalized cell lines.

Among miRNAs, miRNA-21 (miR21) reportedly inhibits apoptosis by targeting PDCD4/AP-1 in infarcted cardiomyocytes [20, 21], and promotes angiogenesis by activating PTEN/Akt signaling and stimulating the expression of vascular endothelial growth factor (VEGF) in endothelial cells [22]. Taking advantages of miRNA-21's anti-apoptosis and angiogenesis-promoting functions, we propose to engineer miRNA-21-enriched EVs derived from serum-starved and genetically modified HEK293T cells, an immortalized cell line commonly used for exosome-producing [23], and then deliver these miR21-loaded EVs (miR21-EVs) through intramyocardial injection to cardiac tissue in hope of promoting cardiac function recovery. Here, we report that these EVs exhibited effective anti-apoptosis activity *in vitro* and *in vivo*, and resulted in high density of arteriole in the infarct area, thus collectively facilitating cardiac function recovery. This EV-mediated delivery of specific miRNAs may be an effective alternative for MI treatment.

Materials and Methods

Reagents

MiR21 expression plasmid (pMIR-miR21) and control miRNA expressed plasmid (pMIR) were purchased from Vigene Biosciences Inc. (China). MiR21 mimic was purchased from RiboBio Co., Ltd. (Guangzhou, China). Computational analysis indicated that miR21 binding site in PDCD4 3'UTR were highly conserved across mouse, rat, and human (**Figure S1**). Lipofectamine® 2000 (Lipo) transfection reagent was provided from Invitrogen (Carlsbad, CA, USA). Linear polyethylenimine (PEI, MW 25k) was purchased from Polyscience Inc. (Warrington, PA, USA). H₂O₂ were purchased from Sinopharm chemical reagent Co., Ltd. (China). BCA Protein Assay Kit was purchased from BioVision (USA). Antibodies against β -actin, cTnI, vWF, CD9, and PDCD4 were purchased from Proteintech Group (China). Antibodies against GOLGA2, CANX, CD63 and CD81 were purchased from ABclonal Biotechnology Co.,Ltd (China). Antibodies against VIM and CD31 were purchased from Cell Signaling Technology, Inc (Danvers, MA, USA). Secondary antibodies were purchased from Jackson ImmunoResearch Inc. (USA). Clarity™ Western ECL substrate was purchased from Bio-Rad Laboratories, Inc. (USA). Hoechst 33258 and DAPI (4',6-diamidino-2-phenylindole) were purchased from Thermo Fisher Scientific Inc. (USA).

TUNEL apoptosis detection kit was purchased from Vazyme Biotech Co., Ltd. (China). PKH26 red fluorescent cell linker kit was purchased from Sigma-Aldrich Co., LLC. (USA). Luciferase Assay System (E1500) was purchased from Promega (Beijing) Biotech Co., Ltd. (China).

Cell culture

Human embryonic kidney cell line (HEK293T), rat heart-derived H9c2 cardiomyoblast cell line and human endothelial cells (HUVECs) were cultured in Dulbecco's modified Eagle's medium (DMEM) supplemented with 10% fetal bovine serum (FBS), 100 U/mL penicillin, and 100 µg/mL streptomycin sulfate. Primary cardiomyocytes (CMs) from mouse neonatal hearts were isolated and maintained as described with modification [24]. Briefly, 1-3 days old neonatal mice were sacrificed by decapitation. The ventricles were immediately excised, quickly minced in ice-cold PBS (Ca²⁺ and Mg²⁺ free) and digested with 0.125% trypsin and 0.05% collagenase type I (Thermo Fisher Scientific Inc.) solution. To enrich for CMs, the cells were preplated for 1.5 hours to remove nonmyocytes. CMs were cultured on collagen-coated tissue culture dishes in cardiac myocyte medium (CMM, ScienCell Research Laboratories Inc.) containing 10% FBS. All cells were maintained in an incubator at 37 °C under 5% CO₂.

Purification of EVs

For generating EVs-encapsulated miRNA, HEK293T cells were transfected with pMIR-miR21 or pMIR. EVs were purified as described previously with modifications [25]. Briefly, after transfection, 293T cells were cultured in DMEM supported with 10% fetal bovine serum at 37 °C with 5% CO₂. Puromycin (2 µg/mL) was used for miRNA-21 or control stable cell line establishment. When reached about 80% confluency, 293T cells were cultured in serum-free DMEM for 48 h. Then supernatants were collected and centrifuged at 300 g for 10 min. To remove cell debris and large vesicles, the supernatants were centrifuged at 12,000 g for 30 min at 4 °C and filtrated with 0.22-µm filter. After this, the sterile supernatants were transferred into sterile polycarbonate bottle and centrifuged at 120,000 g for 70 min at 4 °C using Optima XPN-100 ultracentrifuge (Beckman Coulter, USA) to collect the EVs. After centrifugation, the supernatants were removed and the pellet was resuspended with sterile PBS. Protein content of EVs was measured using BCA Protein Assay Kit.

Transmission electron microscopy (TEM)

For transmission electron microscopy, EVs were fixed in 2% glutaraldehyde in PBS (pH 7.4) overnight.

Then the samples were rinsed in PBS and post-fixed in 1% osmium tetroxide at 4 °C overnight. After dehydrated in increasing concentrations of acetone, samples were embedded in epoxy resin. Ultrathin sections were prepared and adsorbed to formvar-coated copper grids. Samples were stained with uranyl acetate and lead citrate and then observed using Tecnai transmission electron microscope (FEI, USA).

Nanoparticle tracking analysis (NTA)

EVs were diluted with PBS to meet the recommended measurement range (10⁶ to 10⁹ particles/mL) and were analyzed using NanoSight LM10 instruments (Malvern Instruments, Inc., UK). The light scattered by the EVs with laser illumination was captured by a camera and a video file of EVs moving under Brownian motion was created. The NTA software tracked and analyzed particles individually from 10 to 2000 nm and the Stokes-Einstein equation was used to calculate their particle sizes together with an estimate of the concentration [26].

Luciferase assay

3'UTR of mouse PDCD4 was cloned into firefly luciferase vector and the plasmid was co-transfected into 293T cells with pRL-TK Renilla luciferase plasmid. Four hours later, transfected cells were treated with different concentrations of EVs. Cells cultured in 24 well plate were washed with PBS twice and 80 µL lysis reagent was added. All cells were scraped off and transferred into 1.5 mL microcentrifuge tube. After a centrifugation at 12,000g for 15 s, 20 µL supernatants were transferred into a black 96 well plate with flat and clear bottom followed by the supplement of 100 µL luciferase assay reagent. The fluorescence signals were measured immediately using EnSpire® 2300 Multimode Plate Reader (Perkin Elmer Singapore Pte. Ltd., Singapore).

Fluorescence labeling of EVs and internalization of EVs into recipient cells or myocardium

EVs were labeled using PKH26 according to the manufacturer's protocols. H9c2 cells, HUVECs, or CMs were seeded in confocal dishes and cultured overnight. Then the labeled EVs (2 µg/mL) were added. After being incubated at 37 °C with 5% CO₂ for 4 h, cells were washed three times with PBS and then stained using Hoechst 33258 to mark nuclei. To assess EVs uptake by myocardium, 20 µL labeled EVs (1 µg/µL) were injected into the infarct heart of MI mouse. Mice were sacrificed at 1, 2, 4, 8 hours postinjection. The hearts were dehydrated and frozen,

then sliced into 6 μm -thick cryosections on the cross-sections of ventricular papillary muscle regions. The sections were immunofluorescent-stained with anti-cTnI (1:50) or anti-vWF (1:50) and then dyed with Hoechst 33258. The internalization of EVs into recipient cells or myocardium was observed by confocal microscope.

Western blot analysis

Cells or EVs were collected and cells were washed using PBS twice, then cells or EVs were resuspended in 50 μL or 30 μL RIPA Lysis Buffer, respectively. After ultrasound pyrolysis using a Qsonica Q125 sonifier (Qsonica, USA), the lysates were centrifuged and supernatants were collected. Protein concentrations in the supernatants were measured using BCA Protein Assay Kit. Total protein (10-100 μg) was separated in SDS-PAGE and transferred to nitrocellulose membranes. After being blocked with 5% skim milk, membranes were incubated with appropriate primary antibodies, secondary antibodies and ECL substrates in turn. The fluorescence intensity was detected using a BioSpectrum 600 imaging system motorized platform (Ultra-Violet Products Ltd., UK).

RNA isolation, real-time PCR, quantification of miR21 from EVs and RNase resistant rate evaluation

RNA isolation was done as described previously [27]. For quantification of mature miR21, RNA was used to synthesize cDNA using miRNA stem-loop RT primer, and subjected to real-time PCR in a StepOne Plus (Applied Biosystems, USA) using AceQ qPCR SYBR Green Master Mix (Vazyme biotech Co. Ltd., China). Reactions were performed in triplicate, and the miR21 expression was normalized to U6. For quantification of pri-miR21 and pre-miR21, RNA was reverse transcribed to cDNA using the corresponding antisense PCR primer, and the real-time PCR was conducted as described above. The expressions of pri-miR21 and pre-miR21 were normalized to GAPDH or β -actin. Data analyses were done by the comparative Cycle threshold (Ct) method as described previously [27].

To measure miR21 loading content within EVs, a specific miR21 primer provided with a TaqMan® MicroRNA Assay kit (Applied Biosystems) was used. The standard curve of absolute quantification was firstly generated by real-time PCR with different concentrations of synthetic miR21-cDNA standards (10^{-2} μM to 10^{-9} μM). The negative logarithm of these miR21-cDNA concentrations (X axis) were plotted against the Ct values (Y axis). Then miR21 from 2 μg EVs was extracted, reverse transcribed and subjected

to real-time PCR. And the absolute content of miR21 was determined from the generated standard curve. All primers were listed in **Table S1**.

To evaluate RNase resistant rate of some non-viral miRNA delivery systems, miR21 mimic (5 pmol) was diluted in 100 μL serum-free DMEM and then mixed with another 100 μL serum-free DMEM containing 4 μL Lipo or 5 μL PEI. Twenty minutes later RNase (100 $\mu\text{g}/\text{mL}$) was added into the miR21-vector mixture and processed for 30 min at 37 $^{\circ}\text{C}$. MiR21-EVs (20 μg) was also treated under the same condition. Then the amount of remaining miR21 was measured by real-time PCR and the standard curve. RNase resistant rate was calculated by dividing the dosage of remaining miR21 by initial dosage of miR21.

Induction of myocardial infarction, EVs intramyocardial injection and echocardiographic assessment

Eight-week-old male C57BL/6 mice were examined for ejection fraction (EF) by echocardiography and then randomized into 4 groups: receiving sham operation (sham group, $n = 9$), receiving PBS injection after MI (PBS group, $n = 20$), receiving control EVs injection after MI (Ctrl-EVs group, $n = 20$), and receiving miR21 loaded EVs injection after MI (miR21-EVs group, $n = 23$) (**Table S2**). MI was induced by ligating the left anterior descending artery (LAD) as described previously [27]. In brief, mice were anesthetized and intubated and ventilated using a rodent ventilator (Shanghai Alcott Biotech Co., Shanghai, China). Via thoracotomy, the heart was exposed and LAD was blocked using an 8-0 suture. Ischemia was verified by visual inspection and changes in electrocardiography. Sham group underwent the same procedure above excluding the LAD ligation. Then 20 μL EVs (1 $\mu\text{g}/\mu\text{L}$) or PBS were intramyocardial injected into the infarct zone immediately. After injection, the chests were sutured and the animals were looked after with meticulous care. Twenty-four hours after surgery, the cardiac function was evaluated again and mice with EF < 20% or > 50% in MI treated groups were excluded for further study. Specifically, 3 and 4 mice of MI group and miR21-EVs group were dropped out, respectively. Echocardiography assessment showed that EF and fractional shortening (FS) did not differ across three groups, indicating the initial cardiac damage degree are comparable (**Figure S2**). Four weeks after surgery, cardiac function was measured for the last time. In the entire process of the experiment, 19 mice died during the model establishment (6 in the MI group, 9 in the Ctrl-EVs group and 5 in the miR21-EVs group). In addition, 2

mice of MI group died due to cardiac rupture on the 3rd, 4th day after the operation, respectively (Table S2). All animal experimental procedures were approved by Animal Care and Use Committee of the Tongji Medical College, Huazhong University of Science and Technology (Wuhan, China).

Terminal deoxynucleotidyl transferase dUTP nick end labeling (TUNEL) staining, immunohistochemistry and histology

Mice were sacrificed 1 week or 4 weeks after MI. Hearts were embedded in paraffin and the 4- μ m heart cross-sections of ventricular papillary muscle regions were prepared. Sections were blocked and incubated with anti-cTnI (1:50) and apoptotic cells were evaluated by TUNEL staining in the infarcted and peri-infarct zone on myocardial sections of 1 week after MI according to the manufacturer's protocols. Cell nucleus was stained with Hoechst or DAPI. The myocardial sections of 4 weeks were used for blood vessel evaluation and morphologic detection. Blood vessels in the infarct area were determined by quantifying capillaries and arterioles, which were identified using immunostaining for CD31 and α -smooth muscle actin (SMA, 1:100), respectively. The number of blood vessels were counted from 3 random selected fields at the border zone or infarct area according to the experimental needs. The parameters reflecting morphology of infarcted hearts, including infarct size, scar thickness and left ventricular (LV) wall thickness, were calculated as described previously [27]. Polarized light microscopy was used to assess the deposition of collagen I and collagen III. Briefly, 5- μ m paraffin sections were stained using Sirius red. When the collagen fibers were viewed with polarized light, type I collagen fibers exhibit a yellow, orange or red color, whereas type III collagen fibers appeared green [28]. The respective areas of collagen I and collagen III were quantified using the Image-Pro Plus software and the collagen content was expressed as a percentage of the total area of polarized collagen.

Fluorescence *in situ* hybridization (FISH) of miR21

HUVECs were seeded in confocal dishes and cultured overnight. Then miR21-EVs (2 μ g/mL) were added. After being incubated at 37 °C with 5% CO₂ for 4 h, cells were washed three times with PBS and then kept in 4% formalin for 30 min, washed three times with PBS and permeabilized at 4 °C in 70% ethanol overnight. Hybridization with Cy3 labeled or FAM labeled miR21 oligonucleotide probes (Sangon Biotech (Shanghai) Co., Ltd., 8 ng/ μ L) was carried out at 37 °C overnight after incubation in pre-hybridization buffer for 1 h at 37 °C. After three

stringent washes in 2 \times SSC, 1 \times SSC and 0.5 \times SSC, the slides were stained with DAPI.

To assess miR21 in myocardium, 20 μ L miR21-EVs (1 μ g/ μ L) were injected into the infarct heart of wild mouse or C57BL/6-Tg(CAG-EGFP)10sb/J mouse (GFP transgenic mouse, purchased from The Jackson Laboratory). Mice were sacrificed 1 hour after the injection. The hearts were fixed, dehydrated, frozen, and then sliced into 8 μ m-thick cryosections. The sections were digested with proteinase K (20 μ g/mL) at 37 °C for 30 min. The rest of procedure was conducted as described above. To visualize cardiac fibroblasts, the sections were immunofluorescently stained with anti-VIM (1:50) before nuclei staining. The internalization of miR21 into recipient cells or myocardium was observed by confocal microscopy.

Statistical analysis

Statistical differences were calculated through one-way ANOVA analysis using SPSS software (SPSS Inc., USA) in cases of multiple groups. Unpaired student's T-tests were used to compare two groups when appropriate. A value of $p < 0.05$ was considered statistically significant.

Results

Isolation and characterizations of miR21-EVs

To obtain miR21-positive EVs (miR21-EVs), we genetically modified human embryonic kidney cells (HEK293T) to stably express miR21 at a relatively high level. EVs were then harvested from the culture supernatants using ultracentrifugation (Figure 1A) as previously reported [25]. TEM of the isolated pellets showed the bilayer-membrane structure of the vesicles (Figure 1B). NTA revealed that the sizes of 47.2% of miR21-EVs ranged from 30 to 150 nm and its concentration was 4.85×10^{10} particle/mL (Figure 1C). The presence of EV specific proteins (CD9, CD63, and CD81) [29] was verified, while the amount of intracellular proteins, GOLGA2 and CANX, was almost undetectable compared to that of 293T cells, despite loading equal amounts of proteins (Figure 1D). MiR21 level (quantitative PCR) was significantly increased in miR21-EVs than Ctrl-EVs, indicating miR21's high enrichment in miR21-EVs (Figure 1E, black bar). According to the standard curve (Figure S3), miR21 loading content within miR21-EVs was calculated as 36 ± 11 pmol/100 μ g EVs. To determine whether miR21 was encapsulated in the EV's lumen or adhering to the EV's exterior, we treated miR21-EVs with RNase, an enzyme capable of degrading RNA, in the presence of Triton X-100 that could potentially disrupt EV's membrane. RNase treatment alone did not affect the total quantity of

miR21 in the EVs, whereas the further addition of Triton X-100 significantly reduced miR21 level (Figure 1E), indicating that miR21 is physically within the EVs. We further evaluated the RNase resistant rate of miR21-EVs, and compared it with those of commonly used non-viral vectors, such as liposomes (Lipo) and polymeric carriers (PEI). Results showed that miR21 remained basically unchanged in EVs group, but miR21 carried by Lipo or PEI had almost completely degraded (Figure 1F), suggesting EVs may serve as an ideal *in vivo* miRNA delivery vector.

MiR21-EVs efficiently deliver miR21 into recipient cells and reduce PDCD4 protein level *in vitro*

We next determined whether these miR21-loaded EVs could reduce the protein level of PDCD4, a miR21 target gene, in cardiomyocytes and endothelial cells. A reporter plasmid encoding firefly luciferase gene in frame with 3'UTR of mouse PDCD4 (Figure 2A, upper panel) was transfected into 293T cells, which subsequently received a series of concentrations of miR21-enriched EVs. Luciferase expression was significantly reduced when the

concentration was higher than 2 µg/mL (Figure 2A, lower panel). Thus, the concentration of 2 µg/mL miR21-EVs was used for the rest of *in vitro* experiments in this study. To visualize EV uptake, miR21-EVs were labeled with PKH26 dye (labeling cellular plasma membrane) and co-cultured with rat cardiomyoblasts (H9c2), human endothelial cells (HUVECs) and primary cultured neonatal mouse cardiomyocytes (CMs). Most of miR21-EVs was internalized to the perinuclear compartment (Figure 2B and Figure S4). Furthermore, localization of miR21 was examined and visualized using fluorescence *in situ* hybridization (FISH). MiR21 also aggregated at the perinuclear region (Figure S5A) and co-localized with PKH26 dye (Figure S5B). Of note, more than 60% CMs and approximately 90% of H9c2 cells and HUVECs were positive for PKH26 fluorescence after a 4 hours incubation (Figure 2C), indicating that cardiomyocytes and endothelial cells effectively take in miR21-EVs. Since miR21-EVs uptake did not affect the amount of pri- and pre-miR21 (Figure S6), the up-regulated mature miR21 was mainly due to exogenous delivery (Figure 2D).

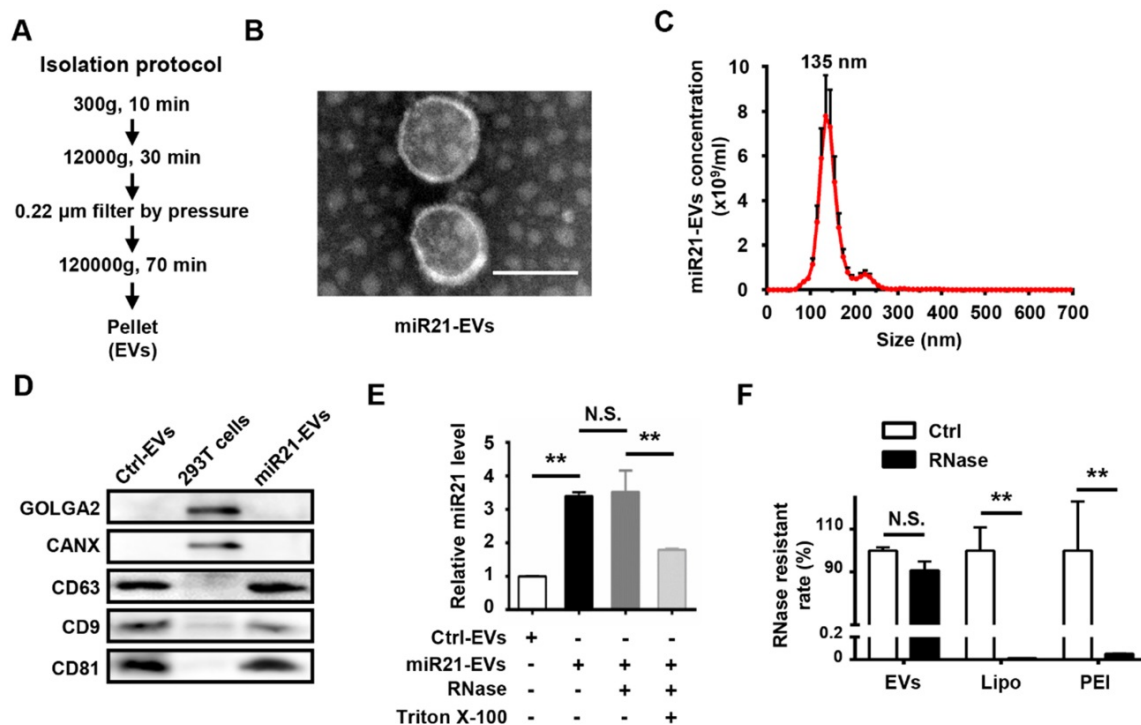


Figure 1. Characterization of EVs from 293T cells. (A) Schematic depiction of the isolation protocol for EVs. (B) Transmission electron microscopy (TEM) images of EVs purified from the supernatants of miR21-transfected 293T cells (miR21-EVs). Scale bar, 100 nm. (C) MiR21-EVs concentration and size distribution determined by NanoSight analysis (NTA). (D) Equal amounts of proteins from whole cells, EVs deprived from the supernatants of 293T cells transfected with pVector (Ctrl-EVs) and miR21-EVs were analyzed by Western blot for the EVs specific proteins, CD9, CD63, and CD81 and intercellular proteins, GOLGA2 and CANX. (E) Determination of relative miR21 level in Ctrl-EVs, miR21-EVs and miR21-EVs treated with RNase or Triton X-100 by qPCR. MiR21-EVs (2 µg) were untreated or treated with RNase (100 µg/mL) or RNase plus 0.1% Triton X-100 under 37 °C for 30 min. A fixed quantity of spike-in cel-miR-39 (25 fmol) was added to each sample before RNA extraction. The retained miR21 expression level was determined by qPCR and normalized to cel-miR-39. (F) RNase resistant rate in miR21-EVs group (EVs), miR21-Lipo group (Lipo), and miR21-PEI group (PEI) after the same treatment as (F). Data shown as mean ± SEM. **, p < 0.01, N.S., not significant.

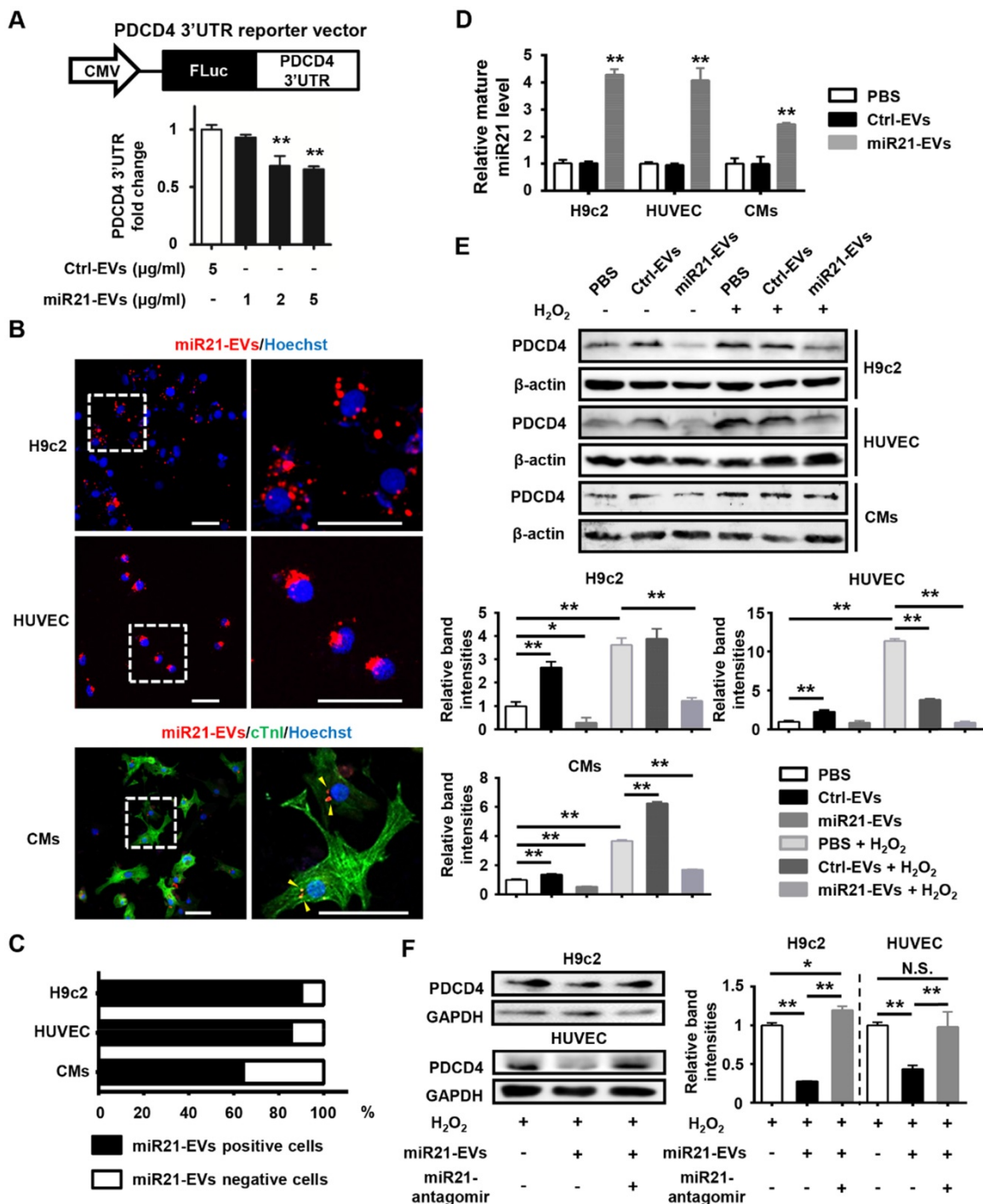


Figure 2. MiR21-loaded EVs are functional in vitro. (A) Schematic representation of pCMV-luc-PDCD4 3'untranslated regions (UTR), the PDCD4 3'UTR reporter vector (upper panel). CMV, cytomegalovirus promoter. FLuc, firefly luciferase. HEK293T cells were co-transfected with pCMV-luc-PDCD4 3'UTR and pRL-TK Renilla luciferase plasmid. Four hours after transfection, the cells were treated with Ctrl-EVs or various doses of miR21-EVs, as indicated. After 24 h, firefly luciferase activity was determined and normalized to Renilla luciferase activity (lower panel). Data shown as mean ± SEM. **, p < 0.01 compared with Ctrl-EVs group. (B) Confocal microscopy images of miR21-EVs uptake by H9c2 cells, HUVECs, and primary cultured neonatal mouse cardiomyocytes (CMs), respectively. MiR21-EVs were labeled with red fluorescent dye PKH26 and incubated with indicated cells for 4 h. The regions boxed with white dashed lines were enlarged on the right. PKH26-labeled miR21-EVs were indicated by yellow arrowheads. Scale bar, 50 µm. (C) Quantification of miR21-EVs positive/negative cells of the corresponding images of (B) (n = 8 per cell line). (D) Analysis of mature miR21 levels by qPCR in H9c2 cells, HUVECs and CMs that were incubated with PBS, Ctrl-EVs or mi21-EVs, respectively, for 12 h. For comparison, miR21 level in PBS group was set as 1. Data shown as mean ± SEM. **, p < 0.01 compared with PBS group. (E) H9c2 cells, HUVECs, and CMs were treated with or without H₂O₂ and simultaneously incubated with PBS, Ctrl-EVs, or miR21-EVs, respectively. (F) H9c2 cells and HUVECs were treated with Ctrl-antagomir or miR21-antagomir (200 nM) in the presence of H₂O₂ and simultaneously incubated with Ctrl-EVs or miR21-EVs, respectively. After 12 h, PDCD4 protein level in (E and F) was determined by Western blot analysis. The working concentration of H₂O₂ was 400 µM in HUVECs and 100 µM in H9c2 cells and CMs, respectively. The ratio of PDCD4 to β-actin or GAPDH (relative band intensity) was measured using the Image-Pro Plus software. Data shown as mean ± SEM. *, p < 0.05, **, p < 0.01, N.S., no significant. The work concentrations of Ctrl-EVs and miR21-EVs were 2 µg/mL in (B-F).

We next examined the effects of miR21-EVs on endogenous PDCD4 protein level in H9c2 cells,

HUVECs and CMs that were subject to induced apoptosis. Hydrogen peroxide (H₂O₂), an exogenous

ROS, was used to trigger oxidative stress-induced cell apoptosis, mimicking cardiomyocyte loss during MI [21]. PDCD4, a pro-apoptosis protein, was upregulated in this process, which however was dampened by miR21-EVs (Figure 2E). We then compared the inhibitory efficiency of PDCD4 between EVs and liposomes. MiR21-EVs dramatically decreased PDCD4 expression 12 hours after incubation in H9c2 cells. However, miR21-mimics delivered by liposomes had no inhibitory effect on PDCD4 in the same space of time (Figure S7). To test whether the inhibitory effect of miR21-EVs depended on miR-21, miR21-antagomir (a small synthetic RNA that constitutively inhibited the activity of miR21) was added along with miR21-EVs. Western blot analysis showed that miR21-antagomir completely reversed the inhibitory effect of miR21-EVs on PDCD4 in H₂O₂-treated H9c2 cells and HUVECs (Figure 2F), suggesting that this inhibitory effect relies on encapsulated miR21. Taken together, these results indicate that miR21-EVs effectively deliver encapsulated miR21 into cardiomyocytes and endothelial cells and reduce PDCD4 protein level, providing a justification for applying miR21-EVs *in vivo* to infarcted cardiac tissue where PDCD4 mediates apoptosis.

Local injected miR21-EVs were rapidly internalized into infarcted myocardium

We then examined the impact of miR21-EVs on the recovery of infarcted hearts (Figure 3A). We first assessed *in vivo* distribution of miR21-EVs in infarcted hearts. The fluorescent microscopy analysis showed that PKH26-labeled miR21-EVs were concentrated in myocardium 1 hour after intramyocardial injection, followed by a gradual outward diffusion over 8 hours (Figure S8A). The qPCR analysis confirmed that miR21-EVs significantly increased miR21 level in infarcted LV myocardium 1, 2, and 4 hours after injection (Figure S8B). To determine whether miR21-EVs were taken up by cardiomyocytes and endothelial cells, immunofluorescent staining for cardiomyocyte-specific (cTnI⁺) and endothelial-specific (vWF⁺) antigens were performed. PKH26-labeled miR21-EVs co-localized with cTnI⁺ cells (Figure 3B) or vWF⁺ cells (Figure 3C) at 48 hours after injection. Notably, FISH analysis showed that concentrated miR21 was found just 1 hour after injection (Figure 3D and F) and predominantly located at the perinuclear region of cardiomyocytes (Figure 3E) and in the cytoplasm of endothelial cells (Figure 3G). Although concentrated miR21 was also detected in cardiac fibroblasts (Figure S9A-B), cardiomyocytes took in much more miR21 than did

fibroblasts (Figure S9C). Together, these results indicate that miR21-EVs are effectively distributed into cardiomyocytes and endothelial cells in infarcted hearts.

Local injection of miR21-EVs efficiently reduces apoptosis in infarcted hearts

PDCD4 is often induced by apoptosis [30]. In light of miR21-EVs reducing PDCD4's protein level *in vitro*, we assessed the anti-apoptosis effect of miR21-EVs *in vivo*. At Week 1 after MI experimentally induced by LAD ligation followed by intramyocardial injection of EVs, the miR21-EVs injection significantly decreased the number of PDCD4 positive cells in infarcted hearts (Figure 4A-B). In addition, the animals receiving miR21-EVs had fewer apoptotic cardiomyocytes (cTnI⁺TUNEL⁺) and apoptotic endothelial cells (CD31⁺TUNEL⁺) in the ischemic border zone compared to those receiving PBS or Ctrl-EVs treatment (Figure 4C-F). These results demonstrate that miR21-EVs effectively inhibit the expression of PDCD4, suppressing apoptosis of cardiomyocytes and endothelial cells *in vivo*. Apart from protecting cardiomyocytes from apoptosis, miR21 also promotes angiogenesis [22]. Four weeks after miR21-EVs treatment, the capillary density (5 to 10 μm in diameter, determined by CD31 immunohistochemical staining) in the ischemic border zone was significantly increased (Figure 4G-H). Interestingly, the arteriole density (determined by SMA immunohistochemical staining) in the infarct area was also increased (Figure 3H-I), indicating that blood vessels can be preserved by miR21-EVs in the infarct zone, probably due to reduced apoptosis of endothelial cells after miR21-EVs treatment.

It has been reported that miR21 enhances cardiac fibroblast survival by inhibiting the expression of its target transcript SPRY1, which leads to ERK-MAP kinase activation, cardiac fibrosis and dysfunction [31]. Thus, we evaluated whether miR21-EVs affect the expression of SPRY1 in myocardium after MI. Immunohistochemistry results showed that SPRY1 positive cells remarkably increased in the border zone at week 1 after MI, but miR21-EVs injection did not increase the numbers of SPRY1 positive cells compared with PBS injection or Ctrl-EVs injection (Figure S10A-B), indicating that miR21-EVs does not affect SPRY1 expression in our therapeutic approach. Taken together, these results reveal miR21-EVs' strong protective effect on myocardium and blood vessels during post-MI cardiac regeneration, which would contribute to a functional recovery.

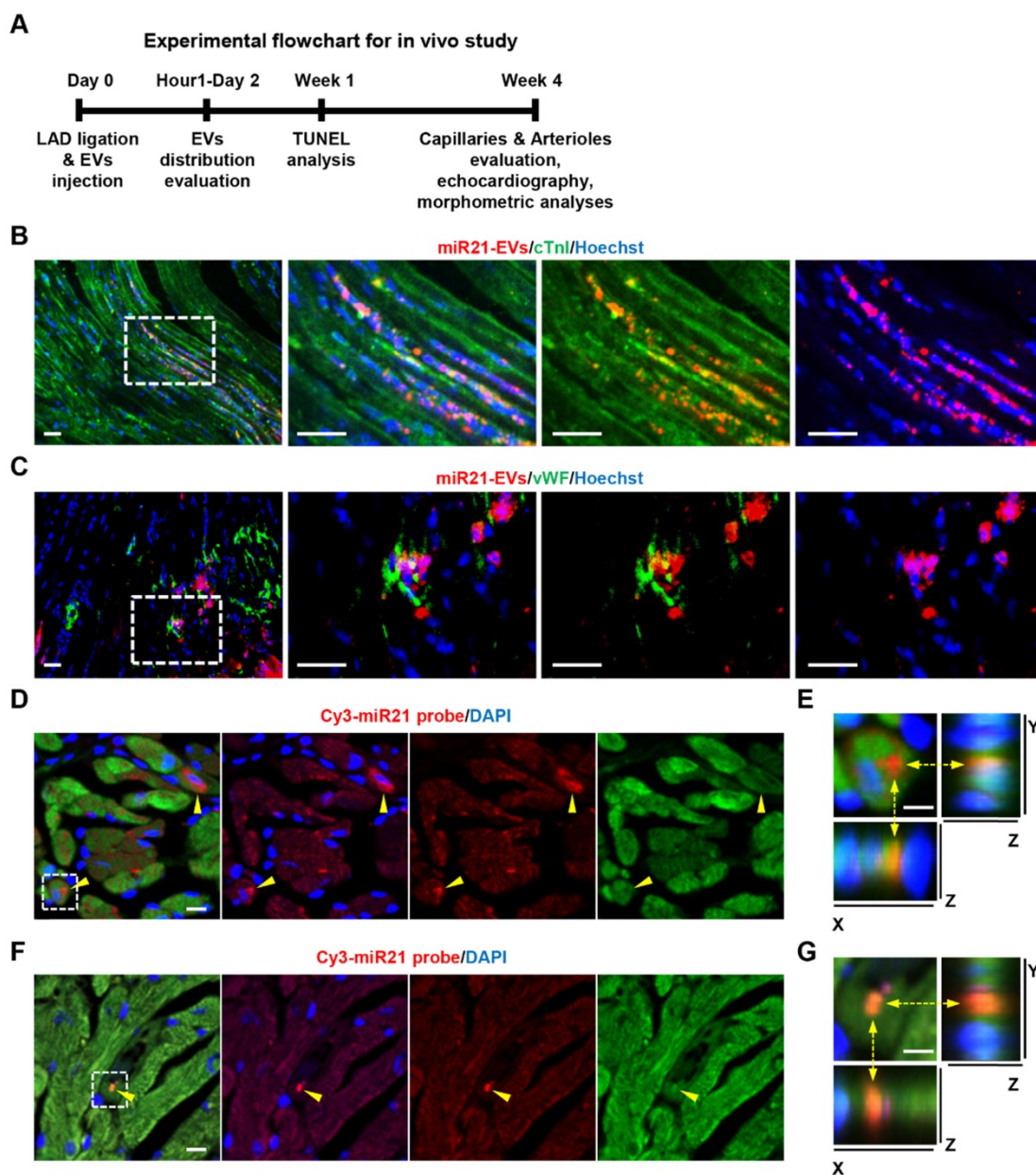


Figure 3. Distribution of miR21-loaded EVs in the mouse infarcted hearts. (A) The flowchart of *in vivo* experimental design and analysis. (B and C) Confocal microscopy images of miR21-EVs taken by cTnI⁺ cardiomyocytes (B) or vWF⁺ endothelial cells (C). PKH26-labeled miR21-EVs were injected into the infarct hearts of MI mice for 48 hours (20 μ g EVs per mouse). The regions boxed with white dashed lines were enlarged in the right panel. Scale bars, 50 μ m. (D and F) FISH analysis in infarcted LV myocardium of GFP-transgenic mice. MiR21-EVs (20 μ g) were injected into the infarct hearts of GFP-transgenic mice. One hour later, cardiomyocytes and endothelial cells were identified based on their morphological characteristics. Cy3-miR21 probe (red) was used to detect miR21. Concentrated miR21 was indicated by yellow arrowheads. Scale bar, 10 μ m. (E and G) The 3D images of corresponding white dashed box in (D) and (F), respectively. The position of Cy3-miR21 probe was indicated by yellow dashed arrows and observed from three perspectives, X-Y plane, X-Z plane and Y-Z plane. Scale bar, 5 μ m.

Intramyocardial injection of miR21-EVs reduces scar formation and improves cardiac function after MI

To explore whether miR21-EVs delivery led to cardiac function recovery after MI, we comprehensively assessed heart histology and cardiac function 4 weeks after MI. While most of myocardium in the infarct zone disappeared after PBS or Ctrl-EVs injection (Figure 5A), viable myocardium was clearly

observed in the infarct zone of the animals receiving miR21-EVs injection. Although miR21-EVs injection had no significant effects on LV wall thickness and infarct size (Figure 5B), it drastically reduced the relative scar thickness (54.03%) compared with PBS injection (72.01%) or Ctrl-EVs injection (74.45%). In addition, we noticed that the deposition of collagen I and collagen III were dramatically increased in the peri-infarct zone after MI (Figure S11A).

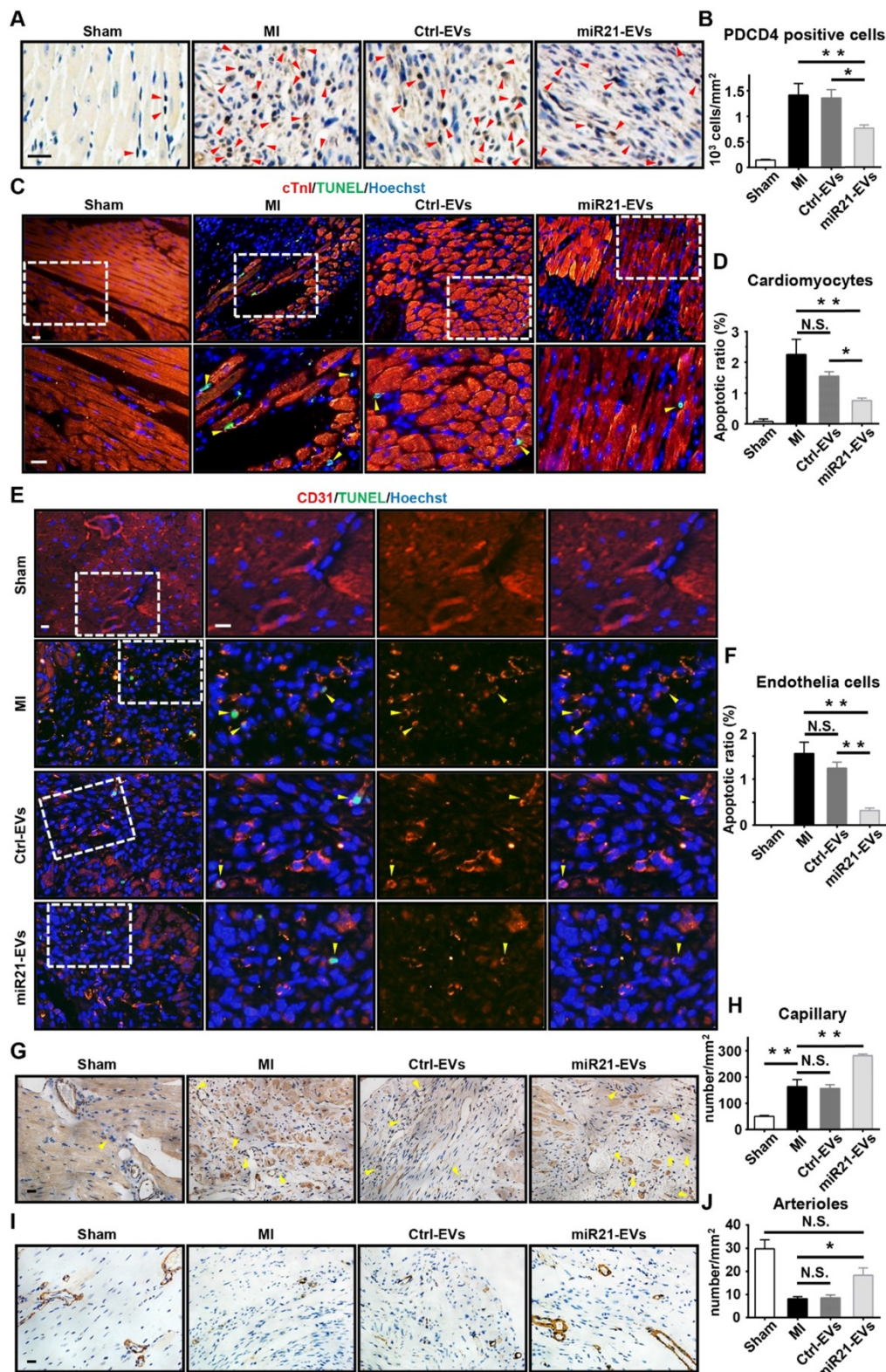


Figure 4. Effect of miR21-loaded EVs in the mouse infarcted hearts. (A) The representative immunohistochemistry images show PDCD4 positive cells in the infarcted hearts of the animals of sham group, MI group or EVs-injected groups 1 week after MI. The PDCD4 positive staining nuclei were indicated by red arrowheads. Scale bars, 20 μ m. (B) Quantification of PDCD4 positive cells of the corresponding images of (A) (4 random fields per animal; n = 3, 3, 3, and 4 for sham group, MI group, Ctrl-EVs group, and miR21-EVs group, respectively). (C and E) TUNEL staining 1 week after acute myocardial infarction and EVs injection into the ischemic center zone. The regions boxed with white dashed lines were enlarged in the lower panel (C) or the right panel (E). The nuclei of apoptotic cardiomyocytes (C) or endothelial cells (E) were indicated by yellow arrowheads. Scale bar, 20 μ m. (D and F) Quantification of cTnI⁺TUNEL⁺ cardiomyocytes (D) or CD31⁺TUNEL⁺ endothelial cells (F) of the corresponding images in (C) or (E), respectively (4 random fields per animal; n = 3, 3, 3, and 4 for sham group, MI group, Ctrl-EVs group, and miR21-EVs group, respectively). (G and I) The representative immunohistochemistry images of CD31 positively stained capillaries (G) at the border zone or SMA positively stained arterioles (I) in the infarct area at week 4 after MI. For sham group, the image of left ventricular were selected. The capillaries (G) were indicated by yellow arrowheads. Scale bar, 20 μ m. (H and J) Quantification of capillary density (H) or arteriole density (J) of the corresponding images of (G) or (I), respectively (3 random fields per animal; n = 3, 5, 4, and 5 for sham group, MI group, Ctrl-EVs group, and miR21-EVs group, respectively). Data shown as mean \pm SEM. *, p < 0.05, **, p < 0.01, N.S., no significant.

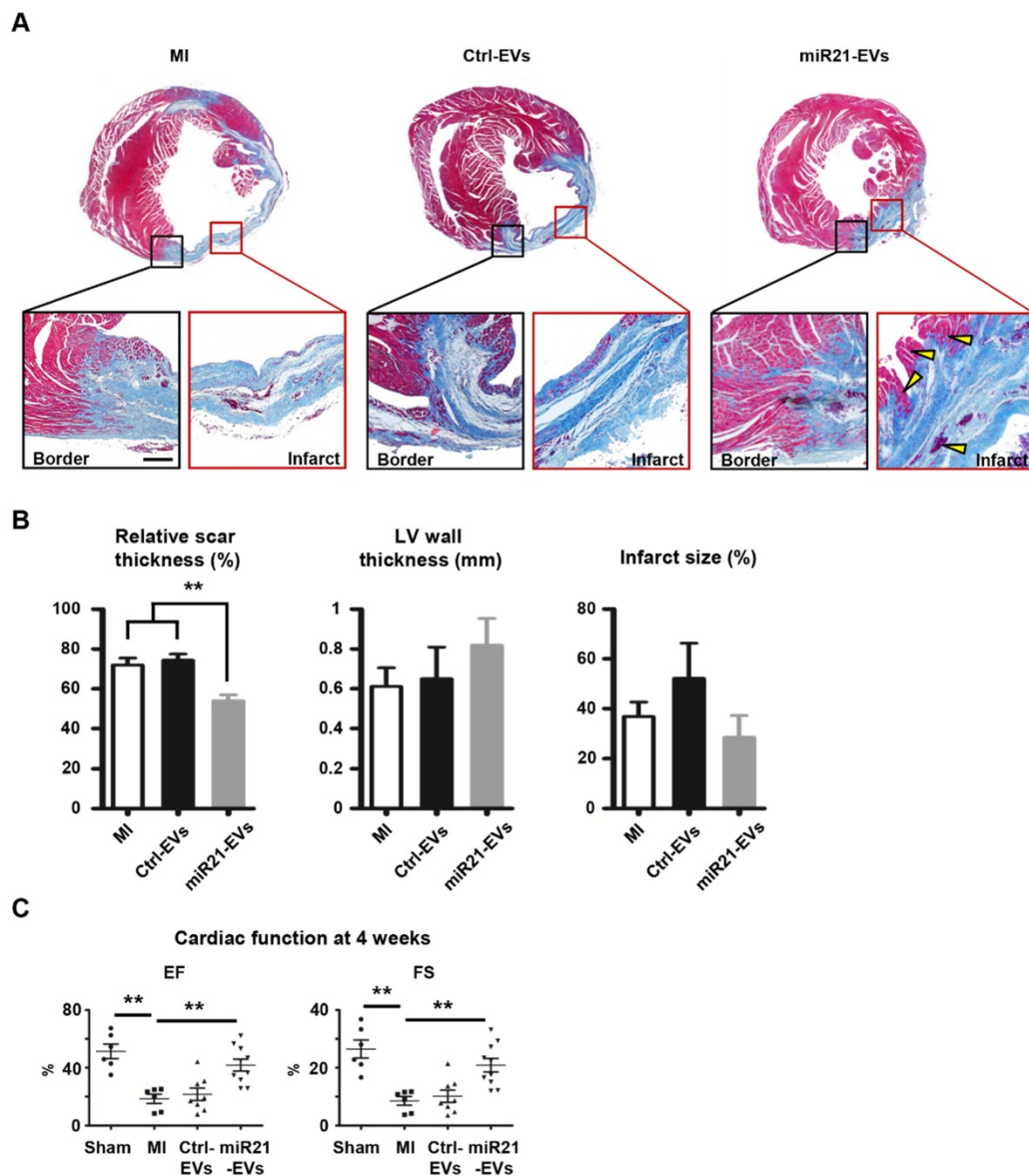


Figure 5. Effect of miR21-loaded EVs on the morphology and cardiac functional recovery of the infarcted hearts. (A) The representative Masson's trichrome stained myocardial cross-sections 4 weeks after acute myocardial infarction with the injection of PBS (MI group), Ctrl-EVs, and miR21-EVs. The regions boxed with black lines (border zone) and red lines (infarct zone) were enlarged below. Viable myocardium was indicated by yellow arrowheads. Scale bar, 200 μ m. (B) Quantification of relative scar thickness, left ventricular (LV) wall thickness, and infarct size in (A) ($n = 6, 4,$ and 6 for MI group, Ctrl-EVs group, and miR21-EVs group, respectively). (C) Ejection fraction (EF) and fractional shortening (FS) were measured by echocardiography at 4 weeks post-MI ($n \geq 6$ per group). Data shown as mean \pm SEM. **, $p < 0.01$.

However, miR21-EVs injection did not increase the content of collagen I or collagen III compared with PBS injection or Ctrl-EVs injection (Figure S11B-C), indicating that miR21-EVs does not affect collagen deposition. Echocardiography showed that EF and FS, two critical indicators reflecting cardiac function, were significantly improved in miR21-EVs injected animals, higher than those in PBS or Ctrl-EVs injected animals (Figure 5C). Consistently, four LV geometrical parameters, including left ventricular end-diastolic dimension (LVEDD), left ventricular end-systolic dimension (LVESD), left ventricular end-diastolic volume (LVEDV), and left ventricular end-systolic volume (LVESV), were significantly decreased in the miR21-EVs group compared with the

MI group, indicating a recovery in ventricular filling and pumping function (Figure S12). Together, these results demonstrate that miR21-EVs injection treatment effectively promotes the cardiac functional recovery.

Considering that miR21-EVs were derived from human cells and used for MI treatment in a mouse model, which might make the therapeutic results ambiguous and bring safety concerns, we explored the relationship between miR21-EVs and inflammation. Firstly, we evaluated the effect of miR21-EVs on the expression of two typical inflammatory genes (TNF- α and IL-1 β) in Raw264.7 mouse macrophages. MiR21-EVs did not activate inflammatory reactions 3 h and 6 h after the treatment

(Figure S13A-B). Secondly, we evaluated the infiltration of macrophages at the peri-infarct zone and found miR21-EVs injection did not promote F4/80⁺ macrophages infiltration at week 1 after MI (Figure S13C-D). Together, these results suggest HEK293T cells derived EVs do not cause inflammation in our research system.

Discussion

MiRNAs have been increasingly investigated as a potential therapeutic agent for treating myocardial injury [32]. A significant obstacle to the miRNA-based treatments is the lack of an efficient and safe delivery system [33]. A variety of approaches, including viral and non-viral delivery systems, have been utilized to inhibit the expression of target genes. In the respect of efficient delivery, viral vectors are the perfect choice. However, safety concerns of viral vectors, such as *in vivo* toxicity, immunogenicity, and tumorigenicity, limit the clinical perspective for the moment, and non-viral approaches seem to be more promising [32, 34]. The delivery efficacy of a carrier system is based on multistep process and inefficiencies at any stage result in a dramatic decrease in gene silencing. Despite this, the majority of studies investigating non-viral vectors focus solely on optimization of endosomal escape [35]. The internalization of lipid nanoparticles and polymeric nanoparticles depends on endocytosis, and they can cause endosomes rupture or leakage that enhances endosomal escape but also leads to the release of cathepsin B, a strong trigger for undesired inflammation and apoptosis [36]. As a novel RNA delivery vehicle, EVs have high efficacy as they delivery cargo directly into the cytosol, bypassing the need for endosomal escape [36]. More importantly, exosomes, a type of EVs with the sizes of 30-150 nm, can deeply penetrate tissues because they can be internalized into the multivesicular bodies (MVB) of recipient cells, then released again to be reinternalized into MVB of secondary recipient cells, and so on. Current non-viral delivery systems, by contrast, only reach the contact layer of tissues thus resulting in poor therapeutic efficacy [37]. Taken together, EV can be regard as an ideal carrier for delivering miRNAs given its biocompatibility, high cellular uptake efficiency and biosafety. Oligonucleotides-loaded EVs have been used to treat various diseases. For example, let-7a miRNA-loaded exosomes inhibited breast cancer progression [38]; opioid receptor mu (MOR) siRNA-loaded exosomes suppressed morphine addiction relapse [39].

Several approaches were used to load EVs with miRNA, such as electroporation and ultrasound sonication. While electroporation generates transient

pores on the bilayer for miRNA loading into EVs, loading efficiency varied widely as it was readily influenced by experimental parameters (voltage and EV concentrations). Similarly, ultrasound sonication induces pore formation on the bilayer for miRNAs to be loaded into EVs, which would damage structural integrity and biological activity of EVs [40]. Further, these two methods require the large amount of miRNA to be synthesized beforehand, which can be costly. Different from these physical loading approaches, genetic modification for generating EVs was inexpensive, convenient, and efficient. After establishment of a miRNA stably-expressing cell line simply by transfecting cells with a miRNA expression plasmid, EVs enriched with a certain miRNA can be rapidly harvested from these cells [25, 41]. Implementing this strategy, we generated miR21-overexpressing 293T cells, a frequently-used cell line for EV-producing [38, 42], which produced EVs with the high abundance of miR21. Given that EVs protected miR21 from RNase-mediated degradation, miR21-containing EVs are RNase-safe. In addition, EV shows its excellent performance in RNase resistance over some commercial and synthetic non-viral miRNA delivery systems (Figure 1F), indicating that EV has congenital advantage in miRNA delivery *in vivo*.

EVs are taken up more efficiently by phagocytic cells than non-phagocytic cells [25]. Murine macrophages (Raw 264.7), a type of phagocytic cells, took up cells-derived exosomes within 4 hours [43], while primary endothelial cells (non-phagocytic cells) needed 24 hours to uptake cell-derived exosomes [44]. Of note, the EV uptake rate in our study appeared to be fast, reaching 90% within just 4 hours in two non-phagocytic cell lines, reflecting the high effectiveness of our cellular delivery approach. It is generally known that the non-viral gene transfer efficiency of primary cardiomyocytes is very poor (typically 5-15% in neonatal cardiomyocytes [24]). Our *in vitro* results showed that more than 60% of neonatal cardiomyocytes took in miR21-EVs within 4 hours. Consistently, the *in vivo* results revealed that concentrated miR21 was detected in cardiomyocytes and endothelial cells of infarcted myocardium just 1 hour after intramyocardial injection. Moreover, a short incubation (<12 h) was sufficient for PDCD4 to be significantly reduced in cardiomyocytes and endothelial cells, indicating miR21-EVs' rapid gene regulatory effect.

The extent of cardiomyocyte loss in the early stages of MI correlates directly with the subsequent decrease of cardiac function. Preventing the loss of cardiomyocytes early is necessary to achieve long-term efficacy in the treatment of ischemic heart

disease [45]. MiR21 can protect cardiomyocytes after MI because of its anti-apoptotic property [21, 46]. Moreover, miR21 promotes angiogenesis by regulating transplanted stem cells and local endothelial cells after MI [22, 47]. Our *in vivo* data showed that miR21-EVs treatment reduced MI-associated cell apoptosis and increased the number of viable cardiomyocytes. Consistent with this observation, miR21-EVs treated mice exhibited a significant cardiac function recovery. A recent study has showed that miR-21 deficiency promoted inflammatory responses in cardiac tissue through targeting KBTBD7 after MI [48], suggesting miR21 may exhibit myocardial protection effects by suppressing inflammation. However, our results showed that miR21-EVs did not inhibit the expression of inflammatory genes in RAW264.7 mouse macrophages and the infiltration of F4/80 positive macrophages at the peri-infarct zone, which may due to the low dosage of miR21-EVs used in our study and the different inhibitory effects of miR21 on different target genes (such as PDCD4 and KBTBD7).

MiR21 is also involved in cardiac fibrosis development by inhibiting other target genes expression. For example, Thum et al. showed that cardiac stress increased miR21 expression, leading to SPRY1 suppression and the followed activation of ERK-MAPK, which played a positive role in cardiac fibroblasts survival and cardiac fibrosis [31]; Roy and colleagues reported that the increased level of miR21 inhibited the PTEN expression in cardiac fibroblasts within the infarct zone after myocardial ischaemia-reperfusion, which induced MMP2 expression and cardiac fibrosis [49]; Liang et al. found that miR21 regulated collagen content by inhibiting TGF β RIII expression and then contributed to cardiac fibrosis after MI [50]. However, Olson's group had come to the contradicted conclusion that miR21 was not essential for cardiac fibrosis from the findings that genetic knockout of miR21 or pharmacological inhibition of miR21 by locked nucleic acid modified anti-miR oligonucleotides did not alter the pathological responses of the heart to cardiac stress including MI [51]. Although the precise role of miR21 in cardiac fibrosis is still debated, there is concern about the possible adverse effects of miR21-EVs therapeutics after MI. Our results showed that miR21-EVs injection did not affect the expression of SPRY1 or the deposition of type I and type III collagen in the peri-infarct zone of MI mice, demonstrating that miR21-EVs does not promote cardiac fibrosis in our treatment strategy. Moreover, our FISH analysis showed that the uptake efficiency of miR21-EVs was significantly higher in cardiomyocytes compared to that in fibroblasts (**Figure S9**), which would reduce

the potential side effects of miR21 in fibroblasts.

There are some limitations in this study which should be commented on. First, although intramyocardial injection is the high-effective route of cardiac gene delivery precisely to the target area, this delivery strategy causes damage and the injected miR21-EVs are likely to leak at the injection spot. Nonetheless, our *in vivo* and *in vitro* data confirm that miR21-EVs are still effectively distributed into myocardium at 48 hours after MI, which are probably due to its ultra-high uptake ratio in cardiomyocytes and endothelial cells. Additionally, our local delivery of miR21-EVs is less possibility to cause side effects because the therapeutic efficacy can be governed at a low dose with reduced systemic side effects. Second, the miR21-EVs can also be taken up by other cell types in heart from lack of targeting ability, which may lead to off-target effects. A targeted delivery strategy to cardiomyocytes by modifying EV's membrane using genetical method or chemical method is an effective approach to resolve the problem. Third, miR21 is a pleiotropic acting miRNA within CVDs, so we have to concern about its pro-fibrogenic effects and other possible side effects. A possible way to overcome this might be a combined use of other microRNAs or drugs.

Conclusions

In summary, we successfully designed and generated miR21-enriched EVs from genetically modified parental cells and comprehensively evaluated their therapeutic efficacy in a mouse infarct model *in vivo*. The EVs protected miR21 against RNase, delivered miR21 into recipient cells efficiently, which in turn significantly decreased PDCD4 protein level, resulting in reduced apoptosis, facilitating cardiac function restoration. This study represents the first study utilizing EVs derived from genetically modified immortalized cells for effective miRNA therapy in the context of MI treatment. The EV-based delivery of exogenous miRNA may be a valuable clinical alternative for myocardial infarction treatment.

Abbreviations

CMs: cardiomyocytes; Ct: Cycle threshold; CVDs: cardiovascular diseases; DMEM: Dulbecco's modified Eagle's medium; EF: ejection fraction; EVs: extracellular vesicles; FS: fractional shortening; HUVEC: human umbilical vein endothelial cell; LAD: left anterior descending artery; LV: left ventricular; LVEDD: left ventricular end-diastolic dimension; LVEDV: left ventricular end-diastolic volume; LVESD: left ventricular end-systolic dimension; LVESV: left ventricular end-systolic volume; MI:

myocardial infarction; miRNAs: microRNAs; miR21: miRNA-21; miR21-EVs: miR21-loaded extracellular vesicles; mRNAs: messenger RNAs; MVB: multivesicular bodies; PDCD4: programmed cell death 4; PEI: polyethylenimine; SMA: α -smooth muscle actin; SPRY1: sprouty homolog 1; TEM: transmission electron microscopy; TUNEL: terminal deoxynucleotidyl transferase dUTP nick end labeling; UTR: untranslated regions.

Supplementary Material

Supplementary figures and tables.

<http://www.thno.org/v09p2346s1.pdf>

Acknowledgements

This work was supported by the National Key Research and Development Program of China (grant number 2016YFA0101100), the National Natural Science Foundation of China Programs (grant numbers 81402875, 81671904, 81572866 and 81773104, 81873931), the International Science and Technology Corporation Program of Chinese Ministry of Science and Technology (grant number 2014DFA32920), the Science and Technology Program of Chinese Ministry of Education (grant number 113044A), the Frontier Exploration Program of Huazhong University of Science and Technology (grant number 2015TS153), the Hundreds of Talents Program of Hubei Province, and the Natural Science Foundation Program of Hubei Province (grant number 2015CFA049), the Advance Research Program of Union Hospital (grant number 02.03.2017-296).

Competing Interests

The authors have declared that no competing interest exists.

References

- Lopez AD, Mathers CD, Ezzati M, Jamison DT, Murray CJ. Global and regional burden of disease and risk factors, 2001: systematic analysis of population health data. *Lancet*. 2006; 367: 1747-57.
- Rao SV, Kaul P, Newby LK, Lincoff AM, Hochman J, Harrington RA, et al. Poverty, process of care, and outcome in acute coronary syndromes. *J Am Coll Cardiol*. 2003; 41: 1948-54.
- Galiuto L, DeMaria AN, Iliceto S. Microvascular damage during myocardial ischemia-reperfusion: pathophysiology, clinical implications and potential therapeutic approach evaluated by myocardial contrast echocardiography. *Ital Heart J*. 2000; 1: 108-16.
- Eefting F, Rensing B, Wigman J, Pannekoek WJ, Liu WM, Cramer MJ, et al. Role of apoptosis in reperfusion injury. *Cardiovasc Res*. 2004; 61: 414-26.
- Mathur A, Martin JF. Stem cells and repair of the heart. *Lancet*. 2004; 364: 183-92.
- Small EM, Frost RJ, Olson EN. MicroRNAs add a new dimension to cardiovascular disease. *Circulation*. 2010; 121: 1022-32.
- Boon RA, Dimmeler S. MicroRNAs in myocardial infarction. *Nat Rev Cardiol*. 2015; 12: 135-42.
- Bartel DP. MicroRNAs: genomics, biogenesis, mechanism, and function. *Cell*. 2004; 116: 281-97.
- Olson EN. MicroRNAs as therapeutic targets and biomarkers of cardiovascular disease. *Sci Transl Med*. 2014; 6: 239ps3.
- Khatiri N, Rathi M, Baradia D, Trehan S, Misra A. In vivo delivery aspects of miRNA, shRNA and siRNA. *Crit Rev Ther Drug Carrier Syst*. 2012; 29: 487-527.

- van Niel G, D'Angelo G, Raposo G. Shedding light on the cell biology of extracellular vesicles. *Nat Rev Mol Cell Biol*. 2018; 19: 213-28.
- Sahoo S, Losordo DW. Exosomes and cardiac repair after myocardial infarction. *Circ Res*. 2014; 114: 333-44.
- De Jong OG, Van Balkom BW, Schiffelers RM, Bouten CV, Verhaar MC. Extracellular vesicles: potential roles in regenerative medicine. *Front Immunol*. 2014; 5: 608.
- Luo Q, Guo D, Liu G, Chen G, Hang M, Jin M. Exosomes from miR-126-overexpressing ADSCs are therapeutic in relieving acute myocardial ischaemic injury. *Cell Physiol Biochem*. 2017; 44: 2105-16.
- Bei Y, Das S, Rodosthenous RS, Holvoet P, Vanhaverbeke M, Monteiro MC, et al. Extracellular vesicles in cardiovascular theranostics. *Theranostics*. 2017; 7: 4168-82.
- Yu B, Kim HW, Gong M, Wang J, Millard RW, Wang Y, et al. Exosomes secreted from GATA-4 overexpressing mesenchymal stem cells serve as a reservoir of anti-apoptotic microRNAs for cardioprotection. *Int J Cardiol*. 2015; 182: 349-60.
- Gray WD, French KM, Ghosh-Choudhary S, Maxwell JT, Brown ME, Platt MO, et al. Identification of therapeutic covariant microRNA clusters in hypoxia-treated cardiac progenitor cell exosomes using systems biology. *Circ Res*. 2015; 116: 255-63.
- Khan M, Nickoloff E, Abramova T, Johnson J, Verma SK, Krishnamurthy P, et al. Embryonic stem cell-derived exosomes promote endogenous repair mechanisms and enhance cardiac function following myocardial infarction. *Circ Res*. 2015; 117: 52-64.
- Wang Y, Zhang L, Li Y, Chen L, Wang X, Guo W, et al. Exosomes/microvesicles from induced pluripotent stem cells deliver cardioprotective miRNAs and prevent cardiomyocyte apoptosis in the ischemic myocardium. *Int J Cardiol*. 2015; 192: 61-9.
- Dong S, Cheng Y, Yang J, Li J, Liu X, Wang X, et al. MicroRNA expression signature and the role of microRNA-21 in the early phase of acute myocardial infarction. *J Biol Chem*. 2009; 284: 29514-25.
- Xiao J, Pan Y, Li XH, Yang XY, Feng YL, Tan HH, et al. Cardiac progenitor cell-derived exosomes prevent cardiomyocytes apoptosis through exosomal miR-21 by targeting PDCD4. *Cell Death Dis*. 2016; 7: e2277.
- Wang K, Jiang Z, Webster KA, Chen J, Hu H, Zhou Y, et al. Enhanced cardioprotection by human endometrium mesenchymal stem cells driven by exosomal microRNA-21. *Stem Cells Transl Med*. 2017; 6: 209-22.
- Tan A, Rajadas J, Seifalian AM. Exosomes as nano-theranostic delivery platforms for gene therapy. *Adv Drug Deliv Rev*. 2013; 65: 357-67.
- Louch WE, Sheehan KA, Wolska BM. Methods in cardiomyocyte isolation, culture, and gene transfer. *J Mol Cell Cardiol*. 2011; 51: 288-98.
- El-Andaloussi S, Lee Y, Lakhali-Littleton S, Li J, Seow Y, Gardiner C, et al. Exosome-mediated delivery of siRNA in vitro and in vivo. *Nat Protoc*. 2012; 7: 2112-26.
- Dragovic RA, Gardiner C, Brooks AS, Tannetta DS, Ferguson DJ, Hole P, et al. Sizing and phenotyping of cellular vesicles using nanoparticle tracking analysis. *Nanomedicine: nanotechnology, biology, and medicine*. 2011; 7: 780-8.
- Song Y, Zhang C, Zhang J, Sun N, Huang K, Li H, et al. An injectable silk sericin hydrogel promotes cardiac functional recovery after ischemic myocardial infarction. *Acta Biomater*. 2016; 41: 210-23.
- Junqueira LC, Cossermelli W, Brentani R. Differential staining of collagens type I, II and III by Sirius Red and polarization microscopy. *Arch Histol Jpn*. 1978; 41: 267-74.
- Simpson RJ, Lim JW, Moritz RL, Mathivanan S. Exosomes: proteomic insights and diagnostic potential. *Expert Rev Proteomics*. 2009; 6: 267-83.
- Shibahara K, Asano M, Ishida Y, Aoki T, Koike T, Honjo T. Isolation of a novel mouse gene MA-3 that is induced upon programmed cell death. *Gene*. 1995; 166: 297-301.
- Thum T, Gross C, Fiedler J, Fischer T, Kissler S, Bussen M, et al. MicroRNA-21 contributes to myocardial disease by stimulating MAP kinase signalling in fibroblasts. *Nature*. 2008; 456: 980-4.
- Kamps JA, Krenning G. Micromanaging cardiac regeneration: Targeted delivery of microRNAs for cardiac repair and regeneration. *World J Cardiol*. 2016; 8: 163-79.
- Gandhi NS, Tekade RK, Chougule MB. Nanocarrier mediated delivery of siRNA/miRNA in combination with chemotherapeutic agents for cancer therapy: current progress and advances. *J Control Release*. 2014; 194: 238-56.
- Marshall E. Gene therapy death prompts review of adenovirus vector. *Science*. 1999; 286: 2244-5.
- Lechardeur D, Lukacs GL. Intracellular barriers to non-viral gene transfer. *Curr Gene Ther*. 2002; 2: 183-94.
- van den Boorn JG, Schlee M, Coch C, Hartmann G. SiRNA delivery with exosome nanoparticles. *Nat Biotechnol*. 2011; 29: 325-6.
- Record M, Subra C, Silvente-Poirot S, Poirot M. Exosomes as intercellular signalosomes and pharmacological effectors. *Biochem Pharmacol*. 2011; 81: 1171-82.
- Ohno S, Takashi M, Sudo K, Ueda S, Ishikawa A, Matsuyama N, et al. Systemically injected exosomes targeted to EGFR deliver antitumor microRNA to breast cancer cells. *Mol Ther*. 2013; 21: 185-91.
- Liu Y, Li D, Liu Z, Zhou Y, Chu D, Li X, et al. Targeted exosome-mediated delivery of opioid receptor Mu siRNA for the treatment of morphine relapse. *Sci Rep*. 2015; 5: 17543.

40. Jiang L, Vader P, Schifflers RM. Extracellular vesicles for nucleic acid delivery: progress and prospects for safe RNA-based gene therapy. *Gene Ther.* 2017; 24: 157-66.
41. Pan S, Yang X, Jia Y, Li R, Zhao R. Microvesicle-shuttled miR-130b reduces fat deposition in recipient primary cultured porcine adipocytes by inhibiting PPAR-g expression. *J Cell Physiol.* 2014; 229: 631-9.
42. Ahmed W, Philip PS, Tariq S, Khan G. Epstein-Barr virus-encoded small RNAs (EBERs) are present in fractions related to exosomes released by EBV-transformed cells. *PLoS One.* 2014; 9: e99163.
43. Feng D, Zhao WL, Ye YY, Bai XC, Liu RQ, Chang LF, et al. Cellular internalization of exosomes occurs through phagocytosis. *Traffic.* 2010; 11: 675-87.
44. Zhou W, Fong MY, Min Y, Somlo G, Liu L, Palomares MR, et al. Cancer-secreted miR-105 destroys vascular endothelial barriers to promote metastasis. *Cancer Cell.* 2014; 25: 501-15.
45. Diwan A, Krenz M, Syed FM, Wansapura J, Ren X, Koesters AG, et al. Inhibition of ischemic cardiomyocyte apoptosis through targeted ablation of Bnip3 restrains postinfarction remodeling in mice. *J Clin Invest.* 2007; 117: 2825-33.
46. Huang W, Tian SS, Hang PZ, Sun C, Guo J, Du ZM. Combination of microRNA-21 and microRNA-146a attenuates cardiac dysfunction and apoptosis during acute myocardial infarction in mice. *Mol Ther Nucleic Acids.* 2016; 5: e296.
47. Zeng YL, Zheng H, Chen QR, Yuan XH, Ren JH, Luo XF, et al. Bone marrow-derived mesenchymal stem cells overexpressing Mir-21 efficiently repair myocardial damage in rats. *Oncotarget.* 2017; 8: 29161-73.
48. Yang L, Wang B, Zhou Q, Wang Y, Liu X, Liu Z, et al. MicroRNA-21 prevents excessive inflammation and cardiac dysfunction after myocardial infarction through targeting KBTBD7. *Cell Death Dis.* 2018; 9: 769.
49. Roy S, Khanna S, Hussain SR, Biswas S, Azad A, Rink C, et al. MicroRNA expression in response to murine myocardial infarction: miR-21 regulates fibroblast metalloprotease-2 via phosphatase and tensin homologue. *Cardiovasc Res.* 2009; 82: 21-9.
50. Liang H, Zhang C, Ban T, Liu Y, Mei L, Piao X, et al. A novel reciprocal loop between microRNA-21 and TGFbetaRIII is involved in cardiac fibrosis. *Int J Biochem Cell Biol.* 2012; 44: 2152-60.
51. Patrick DM, Montgomery RL, Qi X, Obad S, Kauppinen S, Hill JA, et al. Stress-dependent cardiac remodeling occurs in the absence of microRNA-21 in mice. *J Clin Invest.* 2010; 120: 3912-6.